PROGRESS REPORT: APOLLO 17, STATION 6 BOULDER CONSORTIUM*

The Station 6 boulders are derived from a single block which left a distinct track as it rolled from a horizontal belt of boulders down the lower third of North Massif. Subsequently the boulder broke into five large blocks that were sampled (Fig. 1). Maps of the boulders and individual samples, supplemented by petrographic descriptions and photomicrographs, are detailed in reference (1).

Matrices of three of the four units on Fig. 1 were sampled, and each is petrographically distinct. Available data (2) indicate that all matrices have 0.2 - 0.3% K_2O and about 50% feldspar (Table 1); that is the low-K KREEP or high alumina basalt geochemical groups. All matrices form hard crystalline rocks with a wide range in vesicularity.

Unit A was not sampled but is the most vesicular with many vesicles over 5 cm across. The contact between units A and B (sample 76315) has smaller vesicles than unit A and is well-foliated with schlieren-like dark clasts forming color bands parallel to trains of 500 μm dia. vesicles. Its mode is basaltic (Table 1) and texture is generally fine subophitic with some poikilitic bands parallel to the foliation. Matrix feldspars are tabular, rarely exceed 25 μm in length, and cluster about An_{90} in contrast to the feldspar clasts which are more random in composition (Fig. 2). In a test for matrix homogeneity 50 plagioclase grains and about 50 pyroxene and olivine grains in each of nine different areas were analyzed. There was no measurable difference between any of these areas (all results in Fig. 2 and 3). In contrast the composition of 78 pyroxene and olivine mineral clasts are also plotted. The schlieren-like dark clast material is indistinguishable in mineral composition from the matrix material.

Unit B (76015, 76215) is a green-gray poikilitic rock (Table 1) similar to the Apollo 16 poikilitic rocks. It has a well developed foliation, low abundance of clasts and a high content of foliated vesicles, virtually all less than 5 cm across. The matrix consists of a nearly continuous mass of pyroxene oikocrysts each up to 0.2 mm wide and 1 mm long. Feldspar (Fig. 7) occurs as 5-20 μm long laths to subhedral forms mostly enclosed in pyroxene. Fe-Ti oxide with rutile and chromite lamellae occurs between pyroxene oikocrysts as poikilitic grains up to 100 μm enclosing feldspar and phosphate. Irregular, equant to round pores with rare crystals of feldspar and apatite protruding into them form a size continuum to larger, foliated, elongate pores which make up about 15% of the rocks and contain euhedral apatite, troilite, and Fe crystals. Smaller pores about 10 μm across occur between oikocrysts and are bounded by crystal faces of plagioclase and pyroxene. Relic single mineral grains make up about 10% of any sample and have a wider composition spectrum than the matrix which has mineral compositions identical to the matrix of 76315 (Fig. 2 and 3).

Unit C is massive and contains numerous clasts but only a trace of vesicles over 5 cm across. Typical matrix samples (76275, 76295) are blue-grey subophitic rocks (Table 1) with numerous mineral clasts that tend to be concentrated in tan vein-like structures with relatively little melt. Most matrix feldspars are about 10 μm long, less calcic than those of 76315 or 76015 (Fig. 2) and range from euhedral tablets to anhedral forms. Pyroxenes are anhedral, typically about 25 μm across and olivine forms 10 μm anhedral grains. Both are less magnesian than those of 76315 or 76015 (Fig. 3). Fe-Ti oxide occurs as poorly developed plates up to 7 μm across with rutile and spinel lamallae. Metal forms irregular grains about 10 μm across. Pores make up <1-20% (ave. 5%) of the rock as irregular forms 1-10 μm across lacking any well developed protruding crystals. Mineral clasts larger than 10 μm make up 10-15% of the rock. Most are feldspars, some are pyroxene and a few are olivine. Clast compositions are systematically more scattered than matrix compositions (Fig. 2 and 3).

All of the subophitic and poikilitic rocks appear to be crystallized melts. The abundance of round or ovoid vesicles up to 5 cm long contrasts strongly with the angular cavities in metamorphosed Apollo 14 breccias. Additional evidence that the rocks are crystallized melts includes the foliation of dark schlieren and vesicles and the tabular shape of feldspar rather than the granoblastic texture of recrystallized terrestrial and lunar rocks of the same composition.

A poikiloblastic white clast in 76315 containing equant rounded feldspar chadacrysts in oikocrysts of pyroxene has strikingly constant mineral compositions (Fig. 2 and 3). The texture and range of mineral compositions in this material are drastically different than in the poikilitic rocks of unit B and Apollo 16 (3). A granoblastic white rind about 2 to 3 mm thick occurs on one surface of 76315. All minerals again have strikingly constant compositions (Fig. 2 and 3). The unusually high Mg content of this pyroxene is not represented in the pyroxene mineral clasts analyzed in the 9 matrix areas. 76015 contains a large porous clast containing relatively coarse pyroxene and fine plagioclase needles that protrude into pore spaces between the pyroxenes. This clast has not yet been studied in detail.

Samples 76235-39 and 305-307 are friable and broken pieces of a large annealed feldspathic clast in the blue-grey rock, unit C. In contrast to its matrix this clast contains 0.06% K_2O and 27% Al_2O_3

*W. C. Phinney, Consortium Leader, E. Anders, D. Bogard, P. Butler, E. Gibson, W. Gose, G. Heiken, C. Hohenberg, L. Nyquist, W. Pearce, M. Rhodes, L. Silver, C. Simonds, D. Strangway, G. Turner, R. Walker, J. Warner, D. Yuhas

(2). Sample 76230 (from 76235) is an annealed feldspathic rock (Table 1) with a well developed mosaic texture. A few unusually large grains may be relic mineral clasts. Pyroxene occurs as poikilitic grains up to 600 μm long. Olivine forms isolated blebs. All minerals show a very restricted compositional range (Fig. 2 and 3). A second clast in the blue-grey material is 76255 which is a banded tan and white breccia cemented by small amounts of melt. It consists of 100 μm feldspar and inverted pigeonite grains as well as smaller grains of feldspar, pyroxene and olivine. The breccia has irregular pores surrounded by a "matrix" of 20 μm granular pyroxene, olivine and feldspar with small amounts of mesostasis. This complex breccia has not yet been studied in detail but the mineral compositions from 4 thin sections are shown (Fig. 2 and 3).

The variety of lithic clasts, including highly feldspathic varieties and wide range in the composition of feldspar and pyroxene mineral relics, indicates that the KREEP melts were derived from a polymict source, with substantial amounts of material of non-KREEP chemistry. Relic clasts of mare basalt or anorthosites with more than 90% feldspar are totally lacking, indicating that they were not in the protolith. The high percentage of vesicles indicates that the protolith was gas rich, possibly solar wind-rich soil.

Tables 2 adn 3 contain major, trace, isotopic, and model age data for several samples from 76315 and 76015. The homogeneity of the three matrix samples from 76315 and the four matrix samples from 76015 is well shown in both major and trace components. Despite the distinctly different textures of 76315 and 76015 their chemical and mineral compositions are indistinguishable. The dark clast in 76315 has a composition similar to the matrix except for significantly lower K_2O and Rb contents with Rb being even more depleted than K_2O. Analyses of sample 72435 from the South Massif (2) show similar results as the dark clast. The poikiloblastic white clast has the expected major and trace element compositions for its anorthositic gabbro mode (Table 1). The mode of the granoblastic white rind (Table 1) would suggest a higher Al_2O_3 and CaO content than is determined. At first, one might suggest some admixed matrix but the MgO/FeO and TiO_2 values indicate that this is not the case. Perhaps there is enough heterogeneity of mineral distribution in this unit to produce this problem.

The chondrite normalized barium and REE patterns for the matrices and dark clast of these samples are nearly identical and (Fig. 4) fall between the VHA and Apollo 16 KREEP values of Hubbard et al. (5). The typical positive Eu anomaly of anorthositic rocks is shown by 76315,62.

Analyses of siderophile and volatile elements in the matrix and dark clast of 76315 are remarkably similar and suggest, as do most major and trace element data, that these two materials have essentially identical sources (Table 4). On the basis of six diagnostic trace elements, data from all landing sites have been grouped into six distinct clusters (8) presumed to represent the projectiles of six distinct basin forming events. Using the arguments of Morgan (8) the Station 6 boulder samples fall in group 2 and are tentatively assigned to the Serenitatis event (Fig. 5) as are blue-grey breccias with similar meteoritic components from the South Massif and another boulder from North Massif.

Total carbon and sulfur analyses (Table 5) indicate considerable heterogeneity within the matrix of 76015 in contrast to the other major and trace element data. The porous clast was processed with both a band saw and wire saw, and the possibility of both sulfur and carbon contamination is possible. Sulfur is very low and suggests little, if any, contamination, but carbon with the highest value for any lunar breccia may result from some contamination. These variations in both carbon and sulfur make interpretations of single carbon and sulfur analyses in fragmental rocks open to question.

Matrix samples lie on the 4.0 AE whole rock Rb-Sr isochron (Fig. 6) for Apollo 17 noritic breccias (4). The dark clast, 76315,30,C3, falls at the lower extremity of this isochron with Rb-Sr systematics essentially identical to those of 72435 from the South Massif. The white rind, 76315,52, also falls on the isochron but its unusually low trace element abundances raise a question about its relation to the KREEP-rich matrices. The average BABI model age of the foregoing samples is 4.46 ± 0.18 AE. The white clast, 76315,62, falls on the 4.0 AE anorthositic grabbro whole rock isochron and did not acheive isotopic homogenization with the matrix.

Although U-Th-Pb systematics show a limited range of daughter-parent ratios they form nearly concordant systems in the boulder samples (Table 6). Their concentrations fall within the same range as those of the boulders at both stations 2 and 7 (6), indicating that there is little difference between the North and South Massifs. Rake soil 72500 shows similar values (7) suggesting that the soils represent a good average for the massifs despite heterogeneity within the rocks. The relations are unlike most Apollo 16 breccias but quite similar to many Apollo 14 breccias; e.g., 14303 falls in this range. These data are consistent with rocks formed initially at 4.4 to 4.6 AE and metamorphosed at 3.9 to 4.0 AE in agreement with the Rb-Sr data. Except for evidence of terrestrial contamination on 76315,72 exp. 1 which was removed by an acid wash the other $^{235}U/^{204}Pb$ values are very high suggesting that these rocks were largely depleted in common Pb before reaching their present isotopic system. Preliminary results from $^{39}Ar/^{40}Ar$ analyses indicate an age of about 4.1 AE in agreement with both the Rb-Sr and U-Pb systems.

PROGRESS REPORT

PHINNEY et al.

Noble gas data for 76315 (Table 7) indicate Ne and Ar exposure ages of at least 11 to 13 m.y. but are probably low (by up to a factor of two) due to self-shielding effects of the boulder (9). The more direct production rate measurement of a Kr-Kr proton exposure age for this rock gives 21 ± 2 m.y. and is in excellent agreement with a track exposure age (10) of 22 ± 4 m.y. (includes a slight correction of 0.5 mm/m.y. for erosion) (Table 8). This steep track density profile indicates a relatively simple irradiation history for this rock in agreement with the noble gas data (9). It is conceivable that part of the exposure took place before the boulder rolled down the hill. However, the concordancy between track and Kr-Kr ages requires that <2 cm of material could have been removed from the surface of the boulder (in the vicinity of rock 76315) as it rolled down the hill. This seems improbable. The close agreement in ages plus the simple irradiation history suggest that the 21 m.y. age is the time when the boulder rolled down the North Massif.

The Kr-Kr age of sample 76015 is 17.5 ± 1.0 m.y. and is thus distinctly different from that of 76315. This is attributed to a change in shielding of 76015 at some time in the past, i.e., the rate of production of spallation Kr is somewhat higher now than averaged over the entire exposure history. This seems plausible because rock 76015 was perched loosely on the boulder and could not have existed in its present form at the time the boulder rolled down the hill. Gradients of patination and impact pit densities on one surface show that 76015 was cracked apart from the parent rock at some time in the past with the crack surface later being exposed to space. The rare gas samples were taken from this crack surface and it is likely that the increased production rate of spallation isotopes dates from the time the crack occurred.

The track data are consistent with this interpretation. On the rounded side away from the crack surface the initial track gradient (Table 7) is steep and the track exposure age is estimated at 19 m.y. However as the crack surface is approached the gradient suddenly flattens as would be expected if this surface had been exposed suddenly and started to accumulate tracks at a rapid rate. More precise dating of the crack event is underway. A preliminary estimate consistent with the track and rare gas data is that the crack occurred >3 m.y. ago.

Magnetic measurements on 76315 indicate roughly 0.3 wt% metallic Fe almost exclusively as multi-domain (11) indicating a high temperature environment (>900°C). The Station 6 boulder samples exhibit remarkable stability in both direction and intensity. The soft component is conspicuously absent. Essentially all intensities for 76315 are in the 5 x 10^{-6} emu/gm range and for 76015 in the 10^{-5} emu/gm range. Fig. 7 shows the magnetic orientations of 5 chips from 76315 and 5 from 76015. If each rock were uniformly magnetized all directions should coincide. Clearly this is not the case for either rock. Neither uncertainties in orientation nor structural fabric in the rock can account for the non-uniform orientations. In 76015 all samples are matrix material thus ruling out chemical or petrologic variations as the cause. The non-uniformity remains unexplained at this time.

Table 1. Modes(Percent)of Boulder Samples

	Matrix 76315	White clast 76315	White Rind 76315	Matrix 76015	Matrix 76295,76275	Clast 76230
Plagioclase	55	77	76	50	55-60	70
Olivine	22	8	18	3*	6*	10
Orthopyroxene	22	15	7	40	30-35	20
Clinopyroxene			1	4	3	
Fe-Ti oxide	1	<1		3	1	
Metal	<1	<1	Tr	Tr	Tr	
Phosphate				Tr	Tr	
Mesostosis	<1			Tr	Tr	

*Many of these olivines may be small relict clasts

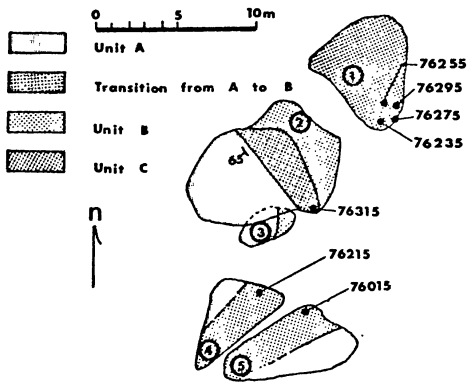

FIGURE 1. Map of Station 6 boulder cluster showing sample locations and lithologic units.

REFERENCES

1. Heiken et al. (1973) NASA TM X-58116, 56 pp.
2. PET (1973) Science, 182, 659-672.
   Apollo 17 Lunar Sample Catalog
3. Simonds et al. (1973) Proc. Fourth Lunar Sci. Conf., 1, 613-632.
4. Hubbard et al. (1973) Proc. Fourth Lunar Sci. Conf., 3, 1297-1312.
5. Morgan et al. (1974) Lunar Science V, 526-528.
   Morgan et al. (1974) Submitted to Soviet-American Conf. on Cosmochem. of Moon and Planets.
6. Nyquist et al. (1974) Lunar Science V, 565-567.
7. Tatsumoto et al. (1974) Lunar Science V, 774-776.
8. Silver (1974) Lunar Science V, 706-708.
9. Bogard et al. (1974) Lunar Science V, 73-75.
10. Walker and Yuhas (1973) Proc. Fourth Lunar Sci. Conf., 3, 2379-2389.
11. Pearce et al. (1974) Lunar Science V, 590-592.

Table 2. Major and selected trace element concentrations for station 6 boulder samples

	Matrix 76315,2	Matrix 76315,35	Matrix next to dark clast 76315,30	Dark Clast 76315,30,3	White Clast 76315,62	White Rind 76315,52	Matrix 76015,22	Matrix 76015,37	Matrix 76015,61	Matrix 76015,64
SiO_2 (wt%)	45.82	46.21	45.64	46.45	45.10	46.57	46.16	46.38	46.38	46.59
TiO_2	1.47	1.50	1.50	1.43	0.36	0.32	1.52	1.55	1.53	1.48
Al_2O_3	18.01	18.14	17.53	18.18	26.37	17.91	17.17	17.78	17.77	18.00
FeO	8.94	8.95	9.53	8.83	5.29	7.66	9.81	9.65	9.07	9.10
MnO	0.11	0.12	0.13	0.13	0.07	0.13	0.13	0.13	0.12	0.12
MgO	12.41	12.02	12.50	12.34	7.46	13.84	13.03	12.40	12.67	12.43
CaO	11.06	11.32	10.97	11.30	15.12	10.36	10.77	11.13	11.11	11.10
Na_2O	0.57	0.60	0.70	0.64	0.47	0.47	-	(0.70*) 0.72	(0.71*) 0.69	(0.70*) 0.75 (0.72*)
K_2O	0.27	0.26	0.26	0.22	0.10	0.15	0.26	0.26	0.26	0.29
P_2O_5	0.29	0.29	0.30	0.29	0.06	0.12	0.27	0.29	0.29	0.28
S	0.08	0.07	0.08	0.07	0.04	0.00	0.09	0.06	0.08	0.08
Cr_2O_3	0.19	0.19	0.19	0.20						
Total	99.22	99.67	99.33	100.08	100.44	99.53	99.91	100.35	99.97	100.22
Sr (ppm)	175	177	174	172						
Rb	5.8	6.2	6.7	3.6						
Y	111	111	113	107						
Zr	510	522	506	478						
Nb	33	33	33	32						
Ni	149									
Zn	4	4	3	2						

Analysts: M. Rhoder, K. Rogers, B. Bansal

*Analyses by H. Wiesmann on same aliquots as in Table 3.

Table 3. Trace Element Concentrations (ppm) and Sr Isotopic Compositions for Station 6 Boulder Samples

	Matrix 76315,2 52.4mg	Matrix 76315,35M 49.2mg	Matrix 76315,30M 51.6mg	Dark Clast 76315,30,C3 66.7mg	White Clast 76315,62 52.5mg	White Rind 76315,52 38.8mg	Matrix 76015,22M 53.2mg	Matrix 76015,37M 53.5mg	Matrix 76015,41M 63.6mg	Matrix 76015,64M 51.5mg
Li	14.6	13.9	15.6	14.1	9.5	11.8	18.3	19.8		
K	2252	2144	2262	1847	809	1244	2223	2304	2279	
Rb	5.88	5.78	6.56	3.85	2.34	3.73	6.41	6.67		
Sr	179.5	174.4	174.8	171.5	153.1	115.2	171.8	177.5	176.6	173.8
Ba	359	337	349	366	72.8	129	348	362	358	354
La	30.1	31.6	32.9	24.7	5.41	7.33	-	34.3	33.4	
Ce	84.6	82.3	84.0	78.6	13.7	18.4	83.3	85.9	84.9	
Nd	53.5	52.7	53.5	50.2	8.60	11.5	52.8	54.4	54.0	
Sm	15.1	14.8	15.1	14.1	2.42	3.20	14.9	15.3	15.2	
Eu	2.00	1.95	1.97	1.88	0.940	0.971	1.94	2.02	1.99	
Gd	18.9	18.8	18.5	17.6	2.99	3.93	18.7	19.0	18.9	
Dy	19.9	19.1	19.7	18.3	3.39	4.59	19.5	20.0	19.9	
Er	11.7	11.4	11.5	11.0	2.14	2.91	11.5	11.8	11.7	
Yb	11.0	10.4	10.6	10.0	2.07	2.98	10.6	11.0	10.8	
Lu										
U	1.52	2.52	1.47	1.36	0.343	0.342	1.46	1.59	1.96	1.48
Th		5.69		5.23			5.44	5.64	5.56	5.41
Cr	1228	1389	1302	1257	770	813	1316			
Zr	477		485	465	95	105	490			
Hf	12.5			11.9	5.3		12.4	12.7		
$^{87}Rb/^{86}Sr$[a]	0.0948±8	0.960±8	0.1084±9	0.0650±6	0.0441±5	0.0937±9	0.1079±9	0.1088±9		
$^{87}Sr/^{86}Sr$[b]	0.70515±5	0.70521±7	0.70595±5	0.70351±10	0.70185±5	0.70491±6	0.70589±9	0.70605±5	0.70589±11	0.70693±6
$T_B(AE)$[c]	4.45±.08	4.44±.08	4.41±.08	4.72±.15	4.35±.13	4.33±.08	4.39±.07	4.45±.07		

[a]Uncertainties correspond to last figures.
[b]Uncertainties correspond to last figures and represent $2\sigma_m$. Normalized
[c]BABI model ages for BABI = 0.6991.

Analysts: L. Nyquist, C. Shih, H. Wiesman, B. Bansal

PROGRESS REPORT

PHINNEY et al.

Table 4. Analysis of 76315 Samples

Element	76315,73 Matrix	76315,74 Dark Clast
Ir ppb	5.42	5.97
Re ppb	0.507	0.575
Au ppb	3.21	3.48
Ni ppm	256	260
Sb ppb	1.49	1.54
Ge ppb	346	354
Se ppb	100	107
Te ppb	3.6	5.1
Ag ppb	0.84	0.88
Br ppb	48	44
Bi ppb	0.098	0.28
Zn ppm	3.1	3.4
Cd ppb	5.0	6.4
Tl ppb	0.31	0.34
Rb ppm	5.91	5.9
Cs ppb	250	250
U ppb	1540	1490

Analysts: E. Anders, J. Morgan

Table 5. Total carbon and sulfur abundances in samples 76015 and 76315

Sample Number	Description	Total Carbon ugC/g	Total Sulfur ugS/g
76315,2	PET sample of matrix	-	755 ± 40
76315,65	Blue-gray matrix of noritic breccia	69 ± 5	785 ± 20
76315,33	Dark-gray clast of noritic breccia	72 ± 5	950 ± 30
76015,32	Matrix with one side exposed to surface	52 ± 5	895 ± 40
76015,58	Matrix from interior	72 ± 5	641 ± 30
76015,59	Matrix from center column	38 ± 7	834 ± 30
76015,65	Martix sample	84 ± 8	680 ± 30
76015,70	Porous clast	214 ± 8	552 ± 30

Analysts: E. Gibson, G. Moore, C. Lewis

Table 7. Noble Gas Concentrations (cm^3 STP/g)

Sample	^3He 10^{-8}	^4He 10^{-5}	^{22}Ne 10^{-8}	^{36}Ar 10^{-8}	^{40}Ar 10^{-5}	^{84}Kr 10^{-10}	^{132}Xe 10^{-10}
76315,34 Matrix	8.24	80.2	2.47	< 26	12.2	12.7	2.27
76315,63 Clast	4.31	9.75	3.88*	3.52	3.97	4.60	1.55
76315,66 Clast	7.01	78.9	4.35*	2.67	12.8	10.5	2.60
76015,60 Matrix	6.61	69.3	1.59	0.82	11.8	2.23	0.31
76015,71 Clast	11.5	28.4	10.5	18.7	19.1	3.54	0.67

Analysts: D. Bogard, W. Hirsch

Table 8. Track vs. Depth Data

76315:

Depth	Track Density
.68 cm	8.6×10^6
1.98 cm	4.52×10^6
3.15 cm	3.16×10^6

76015:

Depth	Track Density
1.3 cm	4.4×10^6
2.4 cm	3.1×10^6
3.5 cm	2.3×10^6
3.7 cm	2.45×10^6
4.3 cm	2.0×10^6
5.0 cm	2.0×10^6
6.3 cm	2.2×10^6
7.3 cm	2.1×10^6 (unoriented clast material)

Analyst: D. Yuhas

Table 6. Contents of U, Th, and Pb and Pb isotopes in station 6 boulder

	exp. 2 Matrix 76015,53	exp. 2 Matrix 76315,71	exp. 1 Dark Clast 76315,72	Acid Washed exp. 1 Matrix Melting ,71	Acid Washed exp. 3 Dark Clast ,72
U ppm	1.495	1.274	0.758	1.084	1.066
Th ppm	5.109	4.192	2.793	3.845	3.494
Pb ppm	3.186	2.760	2.894	2.227	2.339
$^{206}Pb/^{204}Pb$	547.9	799.1	56.79	1925.3	763.2
$^{207}Pb/^{204}Pb$	286.4	397.9	36.93	1084.1	436.8
$^{208}Pb/^{204}Pb$	542.8	752.3	72.37	1782.5	738.0

Analyst: L. Silver

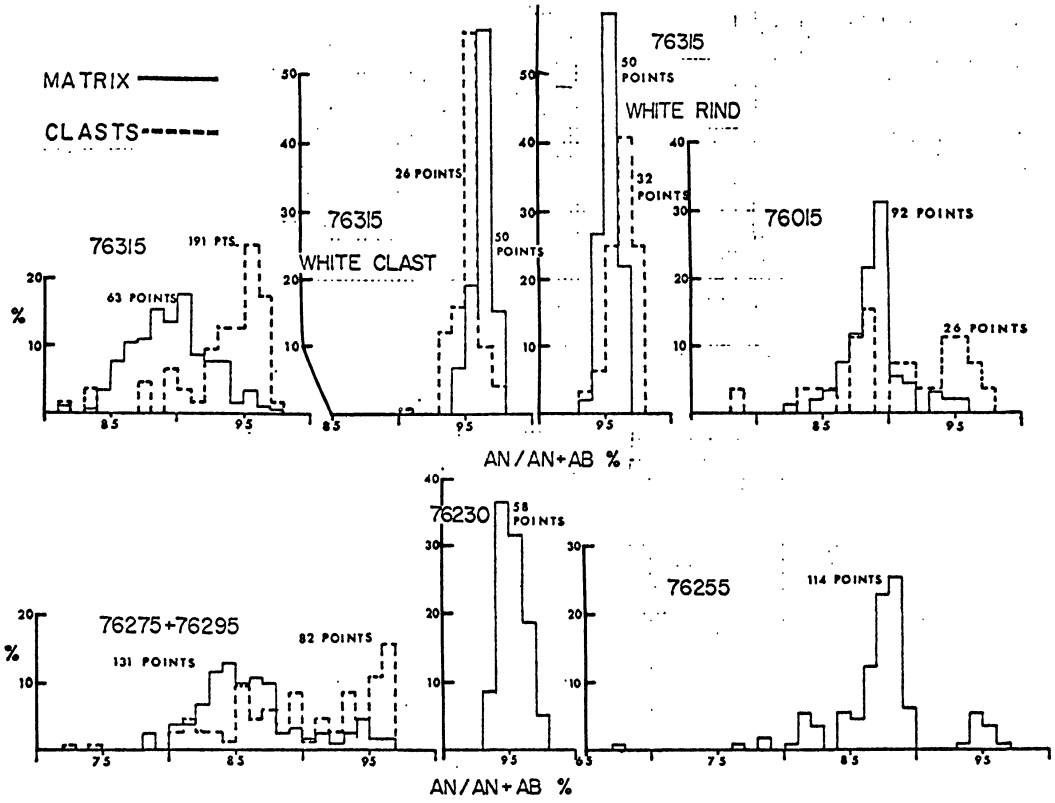

FIGURE 2. Feldspar compositions. (Analysts: Warner & Simonds)

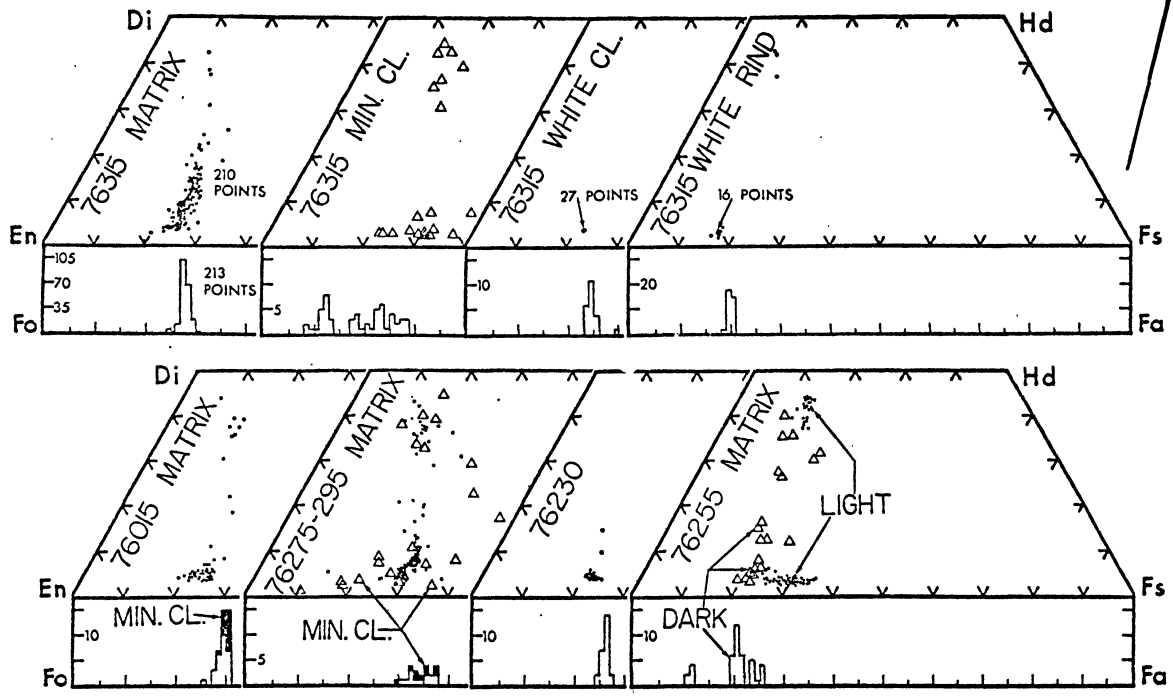

FIGURE 3. Pyroxene and olivine compositions. (Analysts: Simonds & Warner)

PROGRESS REPORT

PHINNEY et al.

FIGURE 4.

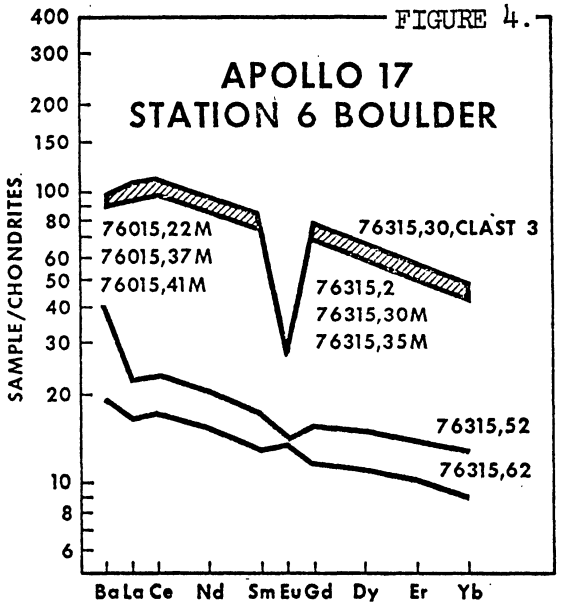

FIGURE 6.

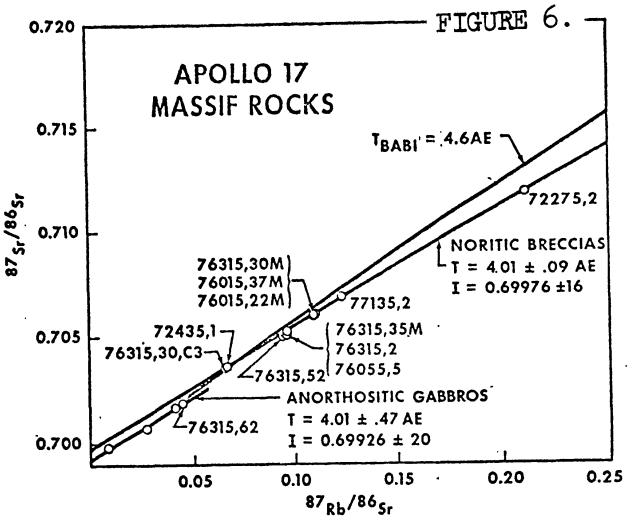

FIGURE 5.

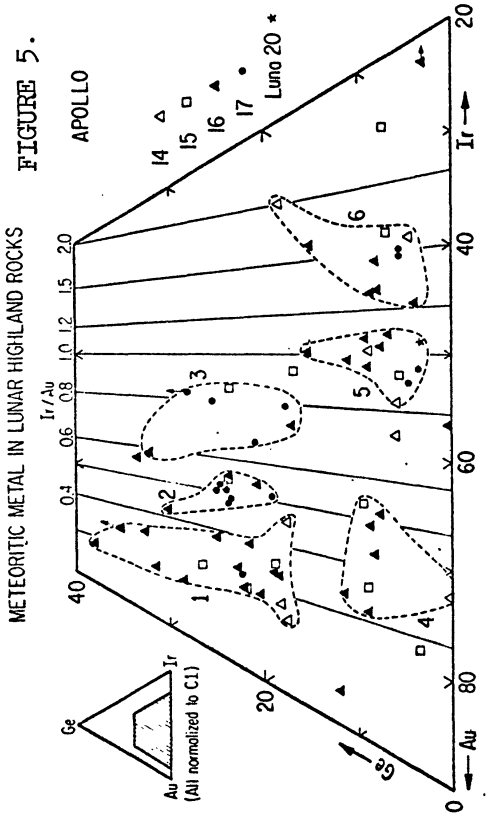

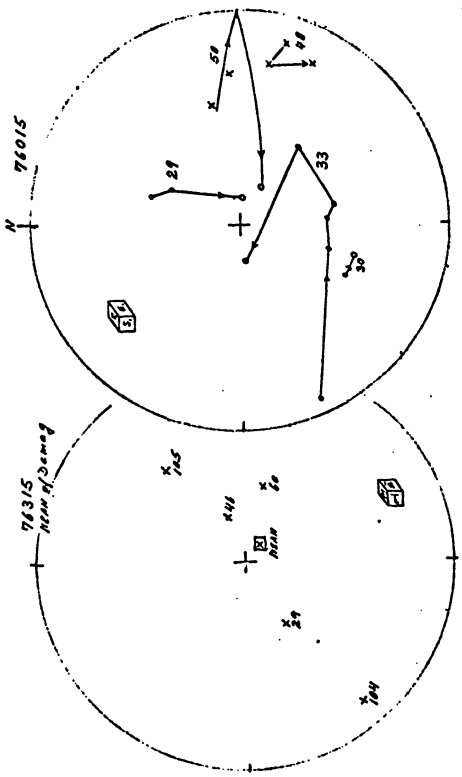

FIGURE 7. Schmidt net projection of directions of magnetization during AF demagnetization (76015) and means (76315). Circles on upper hemisphere, crosses on lower. (analyst: W. Gose).